Topological phases and flat surface bands in superconductors without inversion symmetry

Andreas P. Schnyder[1] and Shinsei Ryu[2]

[1]*Max-Planck-Institut für Festkörperforschung, Heisenbergstrasse 1, D-70569 Stuttgart, Germany*
[2]*Department of Physics, University of California, Berkeley, CA 94720, USA*

(Dated: November 8, 2010)

We examine different topological phases in three-dimensional non-centrosymmetric superconductors with time-reversal symmetry by using three different types of topological invariants. Due to the bulk boundary correspondence, a non-zero value of any of these topological numbers indicates the appearance of zero-energy Andreev surface states. In fully gapped phases the presence of these surface states is independent of the surface orientation, whereas in nodal superconducting phases the Andreev states appear only for certain orientations of the surface. We find that some of these boundary modes in nodal superconducting phases are dispersionless, i.e., they form a flat surface band. These dispersionless Andreev surface bound states have many observable consequences. In particular, they lead to a zero-bias conductance peak in the scanning tunneling spectra.

PACS numbers: 73.43.-f, 73.20.-r, 03.65.Vf, 74.55.+v, 74.45.+c, 73.20.Fz

The hallmark of topological insulators and superconductors (SCs) is the existence of topologically protected conducting boundary modes. The recent experimental observation of these edge and surface states in spin-orbit induced $\mathbb{Z}_2$ topological insulators in two and three dimensions [1, 2], respectively, has lead to a surge of interest and excitement [3, 4]. An exhaustive classification of topologically protected boundary modes occurring in gapped free fermion systems in terms of symmetry and spatial dimension was given in Refs. [5–7]. Interestingly, this classification scheme, which is known as the "periodic table" of topological insulators and SCs, predicts that in three dimensions (3D) there exists a topological SC which satisfies time-reversal symmetry, but breaks spin-rotation symmetry. Indeed, the B phase of ^{3}He is one example of this so-called "class DIII" topological superfluid, whose different topological sectors can be distinguished by an integer topological invariant. Recent ultrasonic attenuation measurements in ^{3}He-B confirmed the existence of the predicted zero-energy surface Majorana bound state [8].

However, finding an electronic analog of the superfluid B phase of ^{3}He remains an outstanding challenge. In this paper we argue that some of the 3D non-centrosymmetric SCs might be examples of electronic topological SCs in symmetry class DIII. We analyze the topological phase diagram of these systems and demonstrate quite generally that adjacent to fully gapped topological phases there exist non-trivial gapless superconducting phases with topologically protected nodal lines (rings). To characterize these gapless lines we introduce a set of topological invariants and show that, due to the bulk-boundary correspondence, the presence of topologically stable nodal rings implies the appearance of dispersionless zero-energy Andreev surface states. These flat surface bands manifest themselves in scanning tunneling measurements as a zero bias conductance peak, a feature which could be used as an experimental signature of the topological non-triviality.

In non-centrosymmetric SCs the absence of inversion in the crystal structure generates antisymmetric spin-orbit (SO) interactions and leads to a mixing of spin-singlet and spin-triplet pairing states. These are the properties that give rise to topologically non-trivial quasi-particle band structures in these systems. Starting with $CePt_3Si$ [9], a multitude of new non-centrosymmetric SCs has recently been discovered, including, among others, $Li_2Pd_xPt_{3-x}B$ [10, 11] $CeRhSi_3$ [12], and Mo_3Al_2C [13].

Model Hamiltonian As a generic phenomenological description applicable to any of the aforementioned materials we employ a single band model with antisymmetric SO coupling and treat superconductivity at the mean field level. Thus, let us consider $\mathcal{H} = \sum_{\boldsymbol{k}} \Psi^\dagger_{\boldsymbol{k}} H(\boldsymbol{k}) \Psi_{\boldsymbol{k}}$ with $\Psi_{\boldsymbol{k}} = (c_{\boldsymbol{k}\uparrow}, c_{\boldsymbol{k}\downarrow}, c^\dagger_{-\boldsymbol{k}\uparrow}, c^\dagger_{-\boldsymbol{k}\downarrow})^T$, where $c^\dagger_{\sigma\boldsymbol{k}}$ is the electron creation operator with spin σ and momentum $\boldsymbol{k}$ and the Bogoliubov-de Gennes (BdG) Hamiltonian is given by

$$H(\boldsymbol{k}) = \begin{pmatrix} h(\boldsymbol{k}) & \Delta(\boldsymbol{k}) \\ \Delta^\dagger(\boldsymbol{k}) & -h^T(-\boldsymbol{k}) \end{pmatrix}. \tag{1a}$$

The normal state Hamiltonian $h(\boldsymbol{k})$ describes non-interacting electrons in a crystal without inversion center

$$h(\boldsymbol{k}) = \varepsilon_{\boldsymbol{k}}\sigma_0 + \boldsymbol{\gamma}_{\boldsymbol{k}} \cdot \boldsymbol{\sigma}, \tag{1b}$$

where $\varepsilon_{\boldsymbol{k}} = \varepsilon_{-\boldsymbol{k}}$ is the spin-independent part of the spectrum, $\sigma_{1,2,3}$ stand for the three Pauli matrices, and σ_0 denotes the 2×2 unit matrix. The second term in $h(\boldsymbol{k})$ represents an antisymmetric SO interaction with pseudovector coupling constant $\boldsymbol{\gamma}_{\boldsymbol{k}}$, which satisfies $\boldsymbol{\gamma}_{-\boldsymbol{k}} = -\boldsymbol{\gamma}_{\boldsymbol{k}}$.

Due to the presence of the parity breaking SO coupling $\boldsymbol{\gamma}_{\boldsymbol{k}}$ the order parameter in Eq. (1a) is in general an admixture of spin-singlet $\psi_{\boldsymbol{k}}$ and spin-triplet $\boldsymbol{d}_{\boldsymbol{k}}$ pairing states

$$\Delta(\boldsymbol{k}) = (\psi_{\boldsymbol{k}}\sigma_0 + \boldsymbol{d}_{\boldsymbol{k}} \cdot \boldsymbol{\sigma})\,(i\sigma_2)\,, \tag{1c}$$

where $\psi_{\boldsymbol{k}}$ and $\boldsymbol{d}_{\boldsymbol{k}}$ are even and odd functions of $\boldsymbol{k}$, respectively. The direction of the spin-triplet component $\boldsymbol{d}_{\boldsymbol{k}}$ is assumed to be parallel to $\boldsymbol{\gamma}_{\boldsymbol{k}}$, as for this choice the antisymmetric SO coupling is not destructive for triplet pairing [14]. Hence, we parametrize the $\boldsymbol{d}$-vector and the SO interaction as $\boldsymbol{d}_{\boldsymbol{k}} = \Delta_t \boldsymbol{l}_{\boldsymbol{k}}$ and $\boldsymbol{\gamma}_{\boldsymbol{k}} = \alpha \boldsymbol{l}_{\boldsymbol{k}}$, respectively. For the spin-singlet component we assume s-wave pairing $\psi_{\boldsymbol{k}} = \Delta_s$ and choose the amplitudes $\Delta_{t,s}$ to be real and positive.

In order to exemplify the topological properties of the BdG Hamiltonian (1), we consider a normal state tight-binding band structure on the cubic lattice $\varepsilon_{\boldsymbol{k}} = t_1(\cos k_x + \cos k_y + \cos k_z) - \mu$, with hopping amplitude

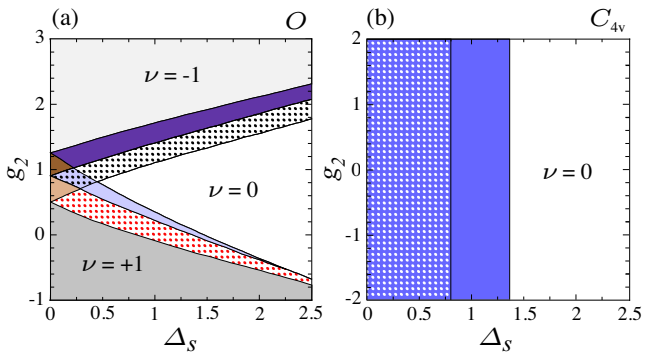

FIG. 1. (color online). Phase diagram as a function of spin-singlet pairing amplitude Δ_s and spin-orbit coupling g_2 [see Eqs. (2) and (3)] for the point group (a) O and (b) C_{4v}. Blue shaded and dotted regions are nodal superconducting phases with $N_{\mathcal{C}_1} = \pm 1$ (red/black dotted), $N_{\mathcal{C}_2} = \pm 1$ (light/dark blue), $N_{\mathcal{C}_3} = +1$ (white dotted), and $N_{\mathcal{C}_4} = +1$ (blue). The gapped phases are characterized by the winding number ν with $\nu = 0$ (white), $\nu = \pm 1$ (dark/light grey), $\nu = -5$ (light brown), and $\nu = +7$ (dark brown).

t_1 and chemical potential μ. We will set $(t_1, \mu, \alpha, \Delta_t) = (4.0, 4.8, 1.0, 1.0)$ henceforth. The specific form of the SO coupling $\boldsymbol{\gamma_k}$ depends on the non-centrosymmetric crystal structure [15], i.e., $g\boldsymbol{\gamma}_{g^{-1}\boldsymbol{k}} = \boldsymbol{\gamma_k}$, where g is any symmetry operation in the point group $\mathcal{G}$ of the crystal. Having in mind $Li_2Pd_xPt_{3-x}B$, we assume for the pseudovector $\boldsymbol{l_k}$ the following form compatible with the symmetry requirements of the cubic point group O

$$\boldsymbol{l_k} = \begin{pmatrix} \sin k_x \\ \sin k_y \\ \sin k_z \end{pmatrix} - g_2 \begin{pmatrix} \sin k_x(\cos k_y + \cos k_z) \\ \sin k_y(\cos k_x + \cos k_z) \\ \sin k_z(\cos k_x + \cos k_y) \end{pmatrix}, \quad (2)$$

with the constant g_2, and where we neglect higher order terms. Furthermore, we also consider the point group C_{4v}, relevant for $CePt_3Si$, in which case $\boldsymbol{l_k}$ reads

$$\begin{aligned} \boldsymbol{l_k} = &(\sin k_y \hat{\boldsymbol{e}}_x - \sin k_x \hat{\boldsymbol{e}}_y) \quad (3) \\ &+ g_2 \sin k_x \sin k_y \sin k_z \,(\cos k_x - \cos k_y)\, \hat{\boldsymbol{e}}_z. \end{aligned}$$

It is important to note that the quasi-particle band topology of $H(\boldsymbol{k})$, as defined by Eq. (1), is mainly determined by the momentum dependence of $\boldsymbol{l_k}$ along the Fermi surface sheets. Hence, the results we obtain are expected to remain qualitatively unchanged upon inclusion of further-neighbor hopping terms in the band structure $\varepsilon_{\boldsymbol{k}}$.

Topological Invariants To characterize the topological properties of $H(\boldsymbol{k})$ we introduce three different topological invariants. But before doing so, we observe that $H(\boldsymbol{k})$ satisfies both time-reversal symmetry (TRS), with $\mathcal{T}^2 = -1$, and particle-hole symmetry (PHS), with $\mathcal{C}^2 = +1$, which are the defining symmetry properties of symmetry class DIII in the terminology of Ref. [5]. Combining TRS and PHS yields a third discrete symmetry, the "chiral" symmetry $\mathcal{S} = \mathcal{TC}$, i.e., there is a unitary matrix $\mathcal{S}$ which anticommutes with $H(\boldsymbol{k})$. It is important to note that while both TRS and PHS relate $H(\boldsymbol{k})$ to $H^T(-\boldsymbol{k})$, $\mathcal{S}$ is a symmetry which is satisfied by $H(\boldsymbol{k})$ at any given point $\boldsymbol{k}$ in the Brillouin zone (BZ).

As shown in Ref. [5] different topological sectors in the fully gapped phases of $H(\boldsymbol{k})$ are distinguished by the class DIII winding number

$$\nu = \int_{\mathrm{BZ}} \frac{d^3k}{24\pi^2} \varepsilon^{\mu\nu\rho} \,\mathrm{Tr}\left[(q^{-1}\partial_\mu q)(q^{-1}\partial_\nu q)(q^{-1}\partial_\rho q)\right], \quad (4)$$

where the integral is over the 1st (BZ) and $q(\boldsymbol{k})$ is the off-diagonal block of the flat-band matrix of $H(\boldsymbol{k})$ [16].

In the nodal superconducting phases the winding number ν is no longer quantized. However, we can consider $H(\boldsymbol{k})$ restricted to 1D loops in reciprocal space and define a topological number in terms of a 1D momentum space loop integral to characterize the topology of the gapless phases. We observe that $H(\boldsymbol{k})$ confined to a generic momentum space loop no longer satisfies TRS nor PHS, but it still obeys chiral symmetry $\mathcal{S}$. Hence, $H(\boldsymbol{k})$ restricted to a loop in the BZ belongs to symmetry class AIII [5] and its topological characteristics are described by the 1D winding number

$$N_{\mathcal{L}} = \frac{1}{2\pi i} \oint_{\mathcal{L}} dl \,\mathrm{Tr}\,[q^{-1}(\boldsymbol{k})\nabla_l q(\boldsymbol{k})], \quad (5)$$

where the integral is evaluated along the loop $\mathcal{L}$ in the BZ. Observe that for *any* closed loop $\mathcal{L}$ that does not intersect with gapless regions in the BZ, $N_{\mathcal{L}}$ is quantized to integer values. If $\mathcal{L}$ is chosen such that it encircles a line node, then $N_{\mathcal{L}}$ determines the topological stability (i.e., the topological charge) of the gapless line [17, 18].

Finally, we also consider $H(\boldsymbol{k})$ restricted to a time-reversal invariant (TRI) loop $\mathcal{L}$, which is mapped onto itself under $\boldsymbol{k} \to -\boldsymbol{k}$. In that case we obtain a 1D Hamiltonian satisfying both TRS and PHS (i.e., belonging to symmetry class DIII). The topological properties of such a 1D system are characterized by the following $\mathbb{Z}_2$ invariant [16]

$$W_{\mathcal{L}} = \prod_{\boldsymbol{K}} \frac{\mathrm{Pf}\left[q^T(\boldsymbol{K})\right]}{\sqrt{\det\left[q(\boldsymbol{K})\right]}}, \quad (6)$$

where $\boldsymbol{K}$ denotes the two TRI momenta on the loop $\mathcal{L}$. Note that $W_{\mathcal{L}}$ is either +1 or -1 for any TRI loop that does not cross gapless regions in the BZ.

Topological Phase diagram Numerical evaluation of the topological numbers (4) and (5) yields the topological phase diagram of $H(\boldsymbol{k})$, which is shown in Fig. 1 as a function of second order SO coupling g_2 and relative strength of singlet and triplet pairing components. Fully gapped phases with different topological properties (i.e., the phases labeled by the winding number $\nu = \pm 1, 0, -5, +7$) are separated in the phase diagram by regions of nodal superconducting phases (blue shaded and dotted areas). The fully gapped phases with $\nu = \pm 1$ are electronic analogs of ^{3}He-B. The nodal superconducting phases exhibit topologically stable nodal rings, which are centered around high symmetry axes of the BZ (see Figs. 2a and 3a). In order to determine the topological character of these nodal lines (and hence of the corresponding gapless phases) it is sufficient to consider the topological invariant

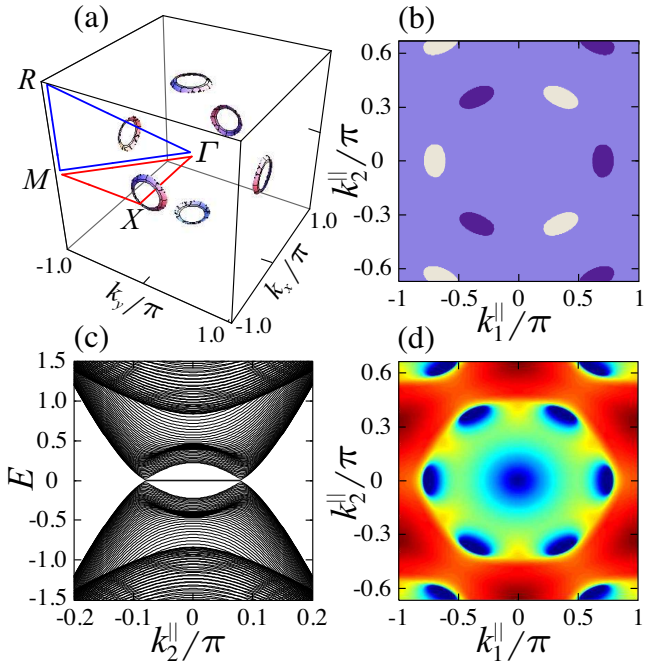

FIG. 2. (color online) Nodal rings (a) and (111) surface states (c,d) for the point group O with $(g_2, \Delta_s) = (0.3, 0.5)$. This parameter choice corresponds to the red dotted region in Fig. 1a. (b) Topological invariant $N_{(111)}$, Eq. (8), as a function of surface momentum $\boldsymbol{k}_\parallel$. Grey and dark blue indicate $N_{(111)} = \pm 1$, while light blue is $N_{(111)} = 0$. (c) Band structure for a slab with (111) face as a function of surface momentum $k_2^\parallel$ with $k_1^\parallel = 0.75\pi$. (d) Energy dispersion of the lowest lying state with positive energy. The color scale is such that dark blue corresponds to zero energy. The states at zero energy in (c) and (d) are localized at the surface. The flat bands in (c) and (d) are singly degenerate (i.e., one branch per surface), whereas the linearly dispersing zero mode at the center of the BZ in (d) is doubly degenerate.

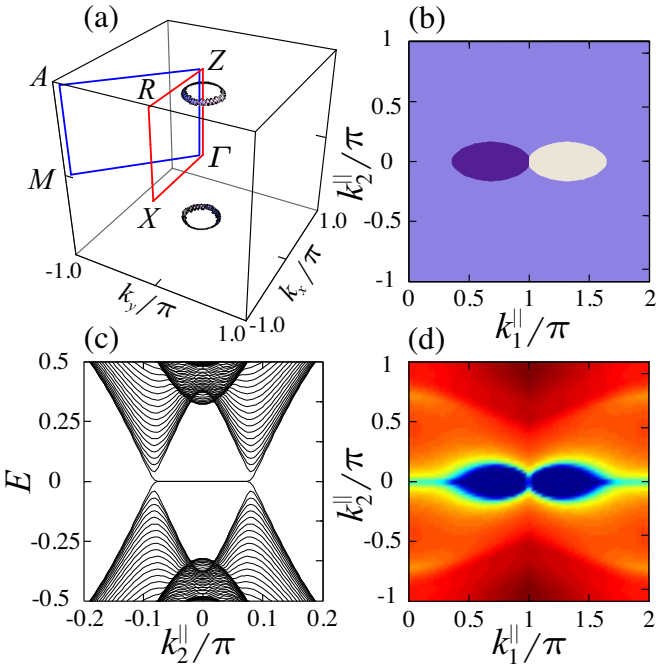

FIG. 3. (color online) Same as Fig. 2 but for the point group C_{4v}, for a slab with (012) face, and with $(g_2, \Delta_s) = (0.0, 0.5)$. This parameter choice corresponds to the white dotted area in Fig. 1b.

$N_\mathcal{L}$ only for loops $\mathcal{L}$ that run along high symmetry axes. Thus, for the cubic point group O we choose the loops as follows

$$\mathcal{C}_1 : \Gamma \to M \to X \to \Gamma, \quad \mathcal{C}_2 : \Gamma \to M \to R \to \Gamma, \quad (7a)$$

whereas for the tetragonal point group C_{4v} we take

$$\begin{aligned} \mathcal{C}_3 &: \Gamma \to Z \to R \to X \to \Gamma, \\ \mathcal{C}_4 &: \Gamma \to Z \to A \to M \to \Gamma. \end{aligned} \quad (7b)$$

For the cubic point group we find that whenever $(N_{\mathcal{C}_1}, N_{\mathcal{C}_2}) = (\pm 1, 0)$ there are topologically stable nodal rings centered around the (100) axis (and symmetry related directions). When $(N_{\mathcal{C}_1}, N_{\mathcal{C}_2}) = (0, \pm 1)$ the gapless lines are oriented along the (111) axis, whereas when $(N_{\mathcal{C}_1}, N_{\mathcal{C}_2}) = (\pm 1, \pm 1)$ the rings are located around the (110) direction. (A similar analysis also holds for the point group C_{4v}.)

Andreev surface states A non-zero quantized value of any of the three topological numbers (4), (5) and (6) implies the existence of zero-energy Andreev surface states. First of all, in fully gapped phases with topologically non-trivial character there appear linearly dispersing Majorana surface modes. This has been discussed previously in the literature [5, 19–21].

In order to understand the appearance of zero-energy Andreev surface states in the gapless phases, we now make use of the topological invariant $N_\mathcal{L}$ with a cleverly chosen loop $\mathcal{L}$. Let us consider Eq. (1) in a slab configuration with (lmn) face. In this geometry the Hamiltonian $H_{(lmn)}$ retains translational invariance along the two independent directions parallel to the (lmn) surface. Hence, $H_{(lmn)}(\boldsymbol{k}_\parallel)$ can be viewed as a family of 1D systems parametrized by the two surface momenta $\boldsymbol{k}_\parallel = (k_1^\parallel, k_2^\parallel)$. Since $H_{(lmn)}(\boldsymbol{k}_\parallel)$ obeys chiral symmetry (but breaks in general TRS and PHS), its topological properties are given by the 1D winding number of class AIII

$$N_{(lmn)}(\boldsymbol{k}_\parallel) = \frac{1}{2\pi i} \int dk_\perp \, \mathrm{Tr} \left[q^{-1}(\boldsymbol{k}) \partial_\perp q(\boldsymbol{k}) \right], \quad (8)$$

where $k_\perp$ is the bulk momentum perpendicular to the surface, and $\partial_\perp = \partial/\partial k_\perp$. Note that $N_{(lmn)}$ is the same as $N_\mathcal{L}$, Eq. (5), with $\mathcal{L}$ chosen along $k_\perp$, following a non-contractible cycle of the BZ torus T^3.

Now, the key observation is that the above line integral is closely related the loop integral $N_\mathcal{L}$, with $\mathcal{L} = \mathcal{C}_i$, that determines the topological charge of the superconducting nodal lines. That is, for those surface momenta $\boldsymbol{k}_\parallel$ for which the loop along $k_\perp$ in Eq. (5) passes through just one non-trivial nodal ring, $N_{(lmn)}(\boldsymbol{k}_\parallel)$ is equal to the topological charge of this given nodal ring. Hence, if we plot $N_{(lmn)}(\boldsymbol{k}_\parallel)$ as a function of surface momenta (see Figs. 2b,3b), we find that the boundaries separating regions with different winding number are identical to the projection of the nodal lines onto the

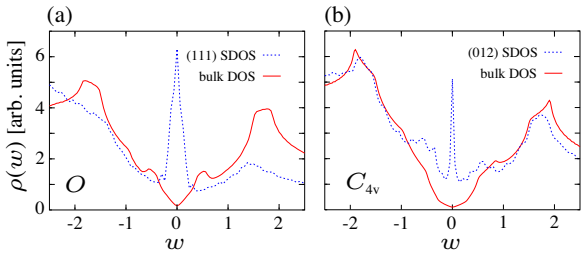

FIG. 4. (color online). Surface and bulk density of states for the point group (a) O and (b) C_{4v}. The surfaces are oriented perpendicular to the (111) and (012) axes, respectively. The employed parameter values are the same as in Figs. 2 and 3.

(lmn) plane. Furthermore, since a non-zero quantized value of $N_{(lmn)}$ implies the existence of zero energy states at the end points of the 1D Hamiltonian $H_{(lmn)}(\boldsymbol{k}_\parallel)$ [5, 22], we find that there are zero-energy Andreev bound states on the (lmn) surface located within the projected nodal rings. This conclusion is corroborated by numerical computations of the zero-energy surface states both for the point group O and C_{4v} (see Figs. 2 and 3). When two nodal rings overlap in the (lmn) projection of the BZ, then the quantized value of $N_{(lmn)}$ in the overlapping region is determined by the additive contribution of the topological charges of the two rings. In particular, one can have a situation where the two contributions cancel, in which case there is no zero-energy surface state within the overlapping region.

Finally, using an analogous argument as in the previous paragraph, we can also employ the $\mathbb{Z}_2$ number (6) to deduce the presence of zero energy modes at TRI momenta of the surface BZ [16]. One example of this is the Kramers pair of surface zero modes located at the center of the surface BZ in Fig. 2d (cf. Refs. [20, 21]). Remarkably, this is a surface Majorana mode in a *gapless* (nodal) superconducting phase [23].

Experimental signatures One of the most direct signatures of the topological aspects of non-centrosymmetric SCs are the surface Andreev bound states. These can be probed by angle-resolved photoemission measurements, or by scanning tunneling spectroscopy (STS) of the surface density of states (SDOS). The bulk density of states of 3D gapless SCs with nodal lines vanishes linearly at zero energy. In contrast, the flat surface bands lead to a diverging zero-energy peak in the SDOS (see Fig. 4), whereas the linearly dispersing Majorana modes located at TRI momenta in the surface BZ generate an additional linear contribution to the tunneling conductance.

The zero-bias peak in the SDOS is strongly dependent on the surface orientation. From this dependence it is in principle possible to (partially) map out the location of the topologically stable nodal lines in the bulk BZ. In addition, one can take advantage of the fact that an applied magnetic field leads to a splitting of the zero-energy peak. Again, this splitting is strongly dependent on the orientation of the magnetic field axis with respect to the nodal lines. Another possibility is to use spatially resolved STS to investigate the SDOS in the presence of impurities on the surface. It is expected that surface impurities will lead to strong spatial modulations of the SDOS, which might give some information about the topological characteristics of the nodal lines in the bulk.

Low-temperature thermal conductivity measurements provide a further experimental tool that could be used to determine the topological characteristics of non-centrosymmetric SCs. While it is in general rather challenging to measure heat transport properties of surface states, thermal conductivity is an excellent probe of the superconducting gap nodes. Hence, by measuring thermal conductivity for different directions of the heat current relative to the orientation of the nodal rings one could obtain indirect information on the topological character of the nodal lines.

In conclusion, using three different topological invariants, we examined the topological properties of general 3D non-centrosymmetric superconductors with TRS. We emphasize that the presented formalism (or a generalization thereof) can be applied to any 3D unconventional SC that preserves TRS. One particularly interesting family of compounds is $Li_2Pd_xPt_{3-x}B$. In these SCs the substitution of Pd by Pt seems to be related to the relative strength of singlet and triplet pairing states [24]. Hence, it might be possible to observe in $Li_2Pd_xPt_{3-x}B$ the transition between two topologically distinct quantum phases as a function of Pt concentration. Another fascinating system is $CePt_3Si$, where experimental measurements point to the existence of line nodes in the order parameter and a large upper critical field H_{c2} indicates spin-triplet pairing [25]. Thus, $CePt_3Si$ might be one of the best candidates for the observation of dispersionless Andreev surface bound states.

Acknowledgments The authors thank B. Béri, A. Furusaki, L. Klam, A. Ludwig, R. Nakai, P. Horsch, and M. Sigrist for discussions. A.P.S. is grateful to the Aspen Center for Physics for hospitality during the preparation of this work. S.R. is supported by Center for Condensed Matter Theory at UC Berkeley.

[1] M. König *et al.*, Science **318**, 766 (2007).
[2] D. Hsieh *et al.*, Nature **452**, 970 (2008).
[3] M. Z. Hasan and C. L. Kane, arXiv:1002.3895.
[4] X.-L. Qi and S.-C. Zhang, arXiv:1008.2026.
[5] A. P. Schnyder, S. Ryu, A. Furusaki, A. W. W. Ludwig, Phys. Rev. B **78** 195125 (2008); AIP Conf. Proc. **1134** 10 (2009).
[6] A. Y. Kitaev, AIP Conf. Proc. **1134** 22 (2009).
[7] S. Ryu, A. P. Schnyder, A. Furusaki, A. W. W. Ludwig, New Journal of Physics **12** 065010 (2010).
[8] S. Murakawa *et al.* Phys. Rev. Lett. **103**, 155301 (2009).
[9] E. Bauer *et al.*, Phys. Rev. Lett. **92**, 027003 (2004).
[10] K. Togano *et al.*,Phys. Rev. Lett. **93**, 247004 (2004).
[11] P. Badica *et al.*, J. Phys. Soc. Jpn. **74**, 1014 (2005).
[12] N. Kimura *et al.*, Phys. Rev. Lett. **95**, 247004 (2005).
[13] E. Bauer *et al.*, arXiv:1007.0420.
[14] P. A. Frigeri *et al.*, Phys. Rev. Lett. **92**, 097001 (2004).

[15] K. V. Samokhin, Annals of Physics **324** 2385 (2009).
[16] See supplementary material for details of the calculation.
[17] B. Béri, Phys. Rev. B **81**, 134515 (2010).
[18] M. Sato, Phys. Rev. B **73** 214502 (2006).
[19] X.-L. Qi *et al.*, Phys. Rev. Lett. **102** 187001 (2009).
[20] A. B. Vorontsov *et al.*, Phys. Rev. Lett. **101**, 127003 (2008).
[21] M. Eschrig, C. Iniotakis, and Y. Tanaka, arXiv:1001.2486.
[22] S. Ryu and Y. Hatsugai, Phys. Rev. Lett. **89**, 077002 (2002).
[23] For a similar Majorana Andreev state at edges of 2D nodal superconductors, see M. Sato and S. Fujimoto, arXiv:1007.4369.
[24] H. Q. Yuan *et al.*, Phys. Rev. Lett. **97**, 017006 (2006).
[25] I. Bonalde *et al.*, Phys. Rev. Lett. **94**, 207002 (2005).

Supplementary Materials

We first discuss basic symmetry properties of superconductors with time-reversal invariance and then go on to derive the topological numbers (4), (5), and (6) from the main text. We shall keep the analysis as general as possible, such that it may be applied to arbitrary superconducting systems. In Section D we will then specialize to the Bogoliubov-de Gennes Hamiltonian (1) describing a single-band non-centrosymmetric superconductor.

Appendix A: Symmetries of the Bogoliubov-de Gennes Hamiltonian

Let us consider a general time-reversal invariant superconductor belonging to symmetry class DIII in the terminology of Refs. [5, 26, 27]

$$H(\boldsymbol{k}) = \begin{pmatrix} h(\boldsymbol{k}) & \Delta(\boldsymbol{k}) \\ \Delta^\dagger(\boldsymbol{k}) & -h^T(-\boldsymbol{k}) \end{pmatrix}, \tag{A1}$$

with the N-band normal state Hamiltonian $h(\boldsymbol{k})$ and the superconducting gap matrix $\Delta(\boldsymbol{k})$, which obeyes $\Delta(\boldsymbol{k}) = -\Delta^T(-\boldsymbol{k})$ because of Fermi statistics. With N bands (orbitals) and two spin degrees of freedom, the total dimension of the Bogoliubov-de Gennes Hamiltonian at momentum $\boldsymbol{k}$ is $4N \times 4N$. A class DIII superconductor satisfies two independent anti-unitary symmetries: time-reversal symmetry $\mathcal{T} = \mathcal{K}U_T$, with $\mathcal{T}^2 = -1$, and particle-hole symmetry $\mathcal{C} = \mathcal{K}U_C$, with $\mathcal{C}^2 = +1$. Here, $\mathcal{K}$ stands for the complex conjugation operator. Time-reversal symmetry constrains $H(\boldsymbol{k})$ as

$$U_T H^*(-\boldsymbol{k}) U_T^\dagger = +H(\boldsymbol{k}), \tag{A2}$$

with $U_T = \mathrm{diag}(u_T, u_T^*)$ and u_T is a $2N \times 2N$ unitary matrix that implements time-reversal invariance of the normal state Hamiltonian, i.e., $u_T h^*(-\boldsymbol{k}) u_T^\dagger = h(\boldsymbol{k})$ and $u_T^T = -u_T$. Observe, Eq. (A2) implies $u_T \Delta^\dagger(\boldsymbol{k}) = \Delta(\boldsymbol{k}) u_T^\dagger$. Particle-hole symmetry acts on the Bogoliubov-de Gennes Hamiltonian $H(\boldsymbol{k})$ as

$$U_C H^*(-\boldsymbol{k}) U_C^\dagger = -H(\boldsymbol{k}), \tag{A3}$$

where $U_C = \sigma_1 \otimes \mathbb{1}_{2N}$, $\sigma_{1,2,3}$ stand for the three Pauli matrices, and $\mathbb{1}_{2N}$ is the $2N \times 2N$ unit matrix. Combining time-reversal and particle-hole symmetry we obtain a third discrete symmetry, which is given by

$$U_S^\dagger H(\boldsymbol{k}) U_S = -H(\boldsymbol{k}), \tag{A4}$$

with $U_S = iU_T U_C$. In other words, there is a unitary matrix U_S that anticommutes with $H(\boldsymbol{k})$ and thereby endows the Hamiltonian with a "chiral" structure. Namely, in the basis in which U_S is diagonal, $H(\boldsymbol{k})$ takes block off-diagonal form

$$\tilde{H}(\boldsymbol{k}) = V H(\boldsymbol{k}) V^\dagger = \begin{pmatrix} 0 & D(\boldsymbol{k}) \\ D^\dagger(\boldsymbol{k}) & 0 \end{pmatrix}, \tag{A5}$$

where the unitary transformation V is given by

$$V = \frac{1}{\sqrt{2}} \begin{pmatrix} \mathbb{1}_{2N} & +iu_T \\ \mathbb{1}_{2N} & -iu_T \end{pmatrix}, \tag{A6}$$

and the block off-diagonal component reads $D(\boldsymbol{k}) = h(\boldsymbol{k}) + i\Delta(\boldsymbol{k}) u_T^\dagger$. In the off-diagonal basis the unitary matrix U_T is given as $\tilde{U}_T = V U_T V^T = \sigma_1 \otimes u_T$. Thus, time-reversal symmetry acts on $D(\boldsymbol{k})$ as follows

$$u_T D^T(-\boldsymbol{k}) u_T^\dagger = D(\boldsymbol{k}). \tag{A7}$$

To compute the $\mathbb{Z}_2$ invariant, Eq. (6), it is advantageous to perform a second basis transformation which brings U_T into the simple form $\bar{U}_T = W U_T W^T = i\sigma_2 \otimes \mathbb{1}_{2N}$. This can be achieved with the help of the unitary matrix $W = \mathrm{diag}(\mathbb{1}_{2N}, u_T)$. In this new basis the Bogoliubov-de Gennes Hamiltonian reads

$$\bar{H}(\boldsymbol{k}) = W \tilde{H}(\boldsymbol{k}) W^\dagger = \begin{pmatrix} 0 & \bar{D}(\boldsymbol{k}) \\ \bar{D}^\dagger(\boldsymbol{k}) & 0 \end{pmatrix}, \tag{A8}$$

with the block off-diagonal component

$$\bar{D}(\boldsymbol{k}) = D(\boldsymbol{k}) u_T^\dagger = h(\boldsymbol{k}) u_T^\dagger - i\Delta(\boldsymbol{k}). \tag{A9}$$

We note that time-reversal symmetry operates on $\bar{D}(\boldsymbol{k})$ as $\bar{D}^T(-\boldsymbol{k}) = -\bar{D}(\boldsymbol{k})$.

Appendix B: Flat Band Hamiltonian and Winding Number

For the derivation of the topological invariants it is convenient to adiabatically deform $H(\boldsymbol{k})$, Eq. (A1), into a flat band Hamiltonian $Q(\boldsymbol{k})$. The only assumptions that we need for computing $Q(\boldsymbol{k})$ are: (i) the Hamiltonian has a full spectral gap and (ii) there is a unitary matrix U_S anticommuting with $H(\boldsymbol{k})$. Thus, the following derivation of $Q(\boldsymbol{k})$ is applicable to any chiral symmetric Hamiltonian with a full bulk gap, in particular also to the three-dimensional topological superconductors in symmetry class AIII, DIII, and CI [5, 7, 28–32].

In what follows, we work in a basis in which $H(\boldsymbol{k})$ takes block off-diagonal form. The flat band Hamiltonian is defined in terms of the projection operator $P(\boldsymbol{k})$ which projects onto filled Bloch eigenstates of $H(\boldsymbol{k})$ at a given momentum $\boldsymbol{k}$. The

projector $P(\boldsymbol{k})$, in turn, is defined in terms of the eigenfunctions of $\tilde{H}(\boldsymbol{k})$

$$\begin{pmatrix} 0 & D(\boldsymbol{k}) \\ D^\dagger(\boldsymbol{k}) & 0 \end{pmatrix} \begin{pmatrix} \chi_a^\pm(\boldsymbol{k}) \\ \eta_a^\pm(\boldsymbol{k}) \end{pmatrix} = \pm\lambda_a(\boldsymbol{k}) \begin{pmatrix} \chi_a^\pm(\boldsymbol{k}) \\ \eta_a^\pm(\boldsymbol{k}) \end{pmatrix}, \quad \text{(B1)}$$

where $a = 1, \ldots, 2N$ is the combined band and spin index. We assume there is a spectral gap around zero energy with $|\lambda_a(\boldsymbol{k})| > 0$, and for definitiveness we choose $\lambda_a(\boldsymbol{k}) > 0$ for all a. Multiplying equation (B1) from the left by $\tilde{H}(\boldsymbol{k})$ yields

$$DD^\dagger \chi_a^\pm(\boldsymbol{k}) = \lambda_a^2 \chi_a^\pm, \quad D^\dagger D \eta_a^\pm = \lambda_a^2 \eta_a^\pm. \quad \text{(B2)}$$

Hence, the eigenfunctions $(\chi_a^\pm, \eta_a^\pm)$ can be obtained from the eigenvectors of $DD^\dagger$ or $D^\dagger D$

$$DD^\dagger u_a = \lambda_a^2 u_a, \quad D^\dagger D v_a = \lambda_a^2 v_a. \quad \text{(B3)}$$

The eigenvectors u_a, v_a are taken to be normalized to one, i.e., $u_a^\dagger u_a = v_a^\dagger v_a = 1$, for all a (here, the index a is not summed over). The eigenstates of $D^\dagger D$ follow from the eigenstates of $DD^\dagger$ via

$$v_a = \mathcal{N}_a D^\dagger u_a, \quad \text{(B4)}$$

with the normalization factor $\mathcal{N}_a$. Using Eq. (B3) one can check that v_a is indeed an eigenvector of $D^\dagger D$,

$$D^\dagger D v_a = D^\dagger D(\mathcal{N}_a D^\dagger u_a) = \mathcal{N}_a \lambda_a^2 D^\dagger u_a = \lambda_a^2 v_a, \quad \text{(B5)}$$

for all a. The normalization factor $\mathcal{N}_a$ is given by

$$u_a^\dagger DD^\dagger u_a = \lambda_a^2 u_a^\dagger u_a = \lambda_a^2 \;\Rightarrow\; \mathcal{N}_a = \frac{1}{\lambda_a}, \quad \text{(B6)}$$

for all a. It follows that the eigenfunctions of $\tilde{H}(\boldsymbol{k})$ are

$$\begin{pmatrix} \chi_a^\pm \\ \eta_a^\pm \end{pmatrix} = \frac{1}{\sqrt{2}} \begin{pmatrix} u_a \\ \pm v_a \end{pmatrix} = \frac{1}{\sqrt{2}} \begin{pmatrix} u_a \\ \pm D^\dagger u_a/\lambda_a \end{pmatrix}. \quad \text{(B7)}$$

With this, the projector $P(\boldsymbol{k})$ onto the filled Bloch states becomes

$$\begin{aligned} P &= \frac{1}{2} \sum_a \begin{pmatrix} u_a \\ -v_a \end{pmatrix} \begin{pmatrix} u_a^\dagger & -v_a^\dagger \end{pmatrix} \quad \text{(B8)} \\ &= \frac{1}{2} \begin{pmatrix} \mathbb{1}_{2N} & 0 \\ 0 & \mathbb{1}_{2N} \end{pmatrix} - \frac{1}{2} \sum_a \begin{pmatrix} 0 & u_a v_a^\dagger \\ v_a u_a^\dagger & 0 \end{pmatrix}. \end{aligned}$$

Finally, we obtain for the flat band Hamiltonian Q, which is defined as $Q = \mathbb{1}_{4N} - 2P$ [5],

$$Q = \sum_a \begin{pmatrix} 0 & u_a v_a^\dagger \\ v_a u_a^\dagger & 0 \end{pmatrix} = \sum_a \begin{pmatrix} 0 & u_a u_a^\dagger \frac{D}{\lambda_a} \\ \frac{D^\dagger}{\lambda_a} u_a u_a^\dagger & 0 \end{pmatrix}. \quad \text{(B9)}$$

In other words, the off-diagonal block of $Q(\boldsymbol{k})$ reads

$$q(\boldsymbol{k}) = \sum_a \frac{1}{\lambda_a(\boldsymbol{k})} u_a(\boldsymbol{k}) u_a^\dagger(\boldsymbol{k}) D(\boldsymbol{k}), \quad \text{(B10)}$$

where $u_a(\boldsymbol{k})$ denotes the eigenvectors of $DD^\dagger$. For a system with completely degenerate bands, $\lambda_a = \lambda$, for all a, the above formula simplifies to

$$q(\boldsymbol{k}) = \frac{1}{\lambda(\boldsymbol{k})} \sum_a u_a(\boldsymbol{k}) u_a^\dagger(\boldsymbol{k}) D(\boldsymbol{k}) = \frac{1}{\lambda(\boldsymbol{k})} D(\boldsymbol{k}). \quad \text{(B11)}$$

Examples of topological insulators and superconductors with completely degenerate bands are the Dirac representatives of Ref. [7].

The integer-valued topological invariant characterizing topological superconductors is now simply given by the winding number of $q(\boldsymbol{k})$. It can be defined in any odd spatial dimension. In three dimensions we have

$$\nu_3 = \int_{\mathrm{BZ}} \frac{d^3k}{24\pi^2} \varepsilon^{\mu\nu\rho} \mathrm{Tr}\left[(q^{-1}\partial_\mu q)(q^{-1}\partial_\nu q)(q^{-1}\partial_\rho q)\right], \quad \text{(B12)}$$

and in one spatial dimension it reads

$$\nu_1 = \frac{1}{2\pi i} \int_{\mathrm{BZ}} dk\, \mathrm{Tr}\left[q^{-1}\partial_k q\right]. \quad \text{(B13)}$$

Appendix C: $\mathbb{Z}_2$ Invariant for Symmetry Class DIII

In this section we compute the $\mathbb{Z}_2$ topological invariant for symmetry class DIII in $d = 1$ and $d = 2$ spatial dimensions. It is most convenient to perform this derivation in the basis (A8), in which the $4N \times 4N$ Bogoliubov-de Gennes Hamiltonian takes the form

$$H(\boldsymbol{k}) = \begin{pmatrix} 0 & D(\boldsymbol{k}) \\ D^\dagger(\boldsymbol{k}) & 0 \end{pmatrix}, \quad D(\boldsymbol{k}) = -D^T(-\boldsymbol{k}). \quad \text{(C1)}$$

In this representation, the time-reversal symmetry operator is given by $\mathcal{T} = \mathcal{K}U_T = \mathcal{K}\, i\sigma_2 \otimes \mathbb{1}_{2N}$ and the flat band Hamiltonian reads

$$Q(\boldsymbol{k}) = \begin{pmatrix} 0 & q(\boldsymbol{k}) \\ q^\dagger(\boldsymbol{k}) & 0 \end{pmatrix}, \quad q(\boldsymbol{k}) = -q^T(-\boldsymbol{k}). \quad \text{(C2)}$$

The presence of time-reversal symmetry allows us to define the Kane-Mele $\mathbb{Z}_2$ invariant [7, 33–37],

$$W = \prod_{\boldsymbol{K}} \frac{\mathrm{Pf}\,[w(\boldsymbol{K})]}{\sqrt{\det[w(\boldsymbol{K})]}}, \quad \text{(C3)}$$

with $\boldsymbol{K}$ a time-reversal invariant momentum. Here, $w(\boldsymbol{k})$ denotes the "sewing matrix"

$$w_{ab}(\boldsymbol{k}) = \langle u_a^+(-\boldsymbol{k}) | \mathcal{T}\, u_b^+(\boldsymbol{k}) \rangle, \quad \text{(C4)}$$

where $a, b = 1, \ldots, 2N$ and $u_a^\pm(\boldsymbol{k})$ is the a-th eigenvector of $Q(\boldsymbol{k})$ with eigenvalue ± 1.

Due to the block off-diagonal structure of Eq. (C2) a set of eigen Bloch functions of $Q(\boldsymbol{k})$ can be constructed as [7]

$$|u_a^\pm(\boldsymbol{k})\rangle_{\mathrm{N}} = \frac{1}{\sqrt{2}} \begin{pmatrix} n_a \\ \pm q^\dagger(\boldsymbol{k}) n_a \end{pmatrix}, \quad \text{(C5)}$$

or, alternatively, as

$$|u_a^\pm(\boldsymbol{k})\rangle_{\mathrm{S}} = \frac{1}{\sqrt{2}} \begin{pmatrix} \pm q(\boldsymbol{k}) n_a \\ n_a \end{pmatrix}, \quad \text{(C6)}$$

where n_a are $2N$ momentum independent orthonormal vectors. For simplicity we choose $(n_a)_b = \delta_{ab}$. In passing, we

note that both $|u_a^{\pm}(\boldsymbol{k})\rangle_{\rm N}$ and $|u_a^{\pm}(\boldsymbol{k})\rangle_{\rm S}$ are well-defined globally over the entire Brillouin zone. To compute the $\mathbb{Z}_2$ topological number we choose the basis $|u_a^{\pm}(\boldsymbol{k})\rangle_{\rm N}$. Combining Eqs. (C4) and (C5) yields

$$\begin{aligned} w_{ab}(\boldsymbol{k}) &= \frac{1}{2}\begin{pmatrix} n_a^\dagger, & n_a^\dagger q(-\boldsymbol{k}) \end{pmatrix} i\sigma_2\otimes \mathbb{1}_{2N}\mathcal{K}\begin{pmatrix} n_b \\ q^\dagger(\boldsymbol{k})n_b \end{pmatrix} \\ &= \frac{1}{2}\begin{pmatrix} n_a^\dagger, & n_a^\dagger q(-\boldsymbol{k}) \end{pmatrix}\begin{pmatrix} q^T(\boldsymbol{k})n_b \\ -n_b \end{pmatrix} \\ &= \frac{1}{2}\left(n_a^\dagger q^T(\boldsymbol{k})n_b - n_a^\dagger q(-\boldsymbol{k})n_b\right) \\ &= q_{ab}^T(\boldsymbol{k}). \end{aligned} \tag{C7}$$

In the second last line we used Eq. (C2), i.e., $q(-\boldsymbol{k}) = -q^T(\boldsymbol{k})$. In conclusion, the $\mathbb{Z}_2$ topological number in spatial dimensions $d=2$ and $d=1$ is given by

$$W = \prod_{\boldsymbol{K}} \frac{\mathrm{Pf}\,\left[q^T(\boldsymbol{K})\right]}{\sqrt{\det\left[q(\boldsymbol{K})\right]}}, \tag{C8}$$

where $\boldsymbol{K}$ denotes the four (two) time-reversal invariant momenta of the two-dimensional (one-dimensional) Brillouin zone.

Appendix D: Flat Band Hamiltonian for the Non-centrosymmetric Superconductor, Eq. (1)

Let us now apply the formalism developed in the preceding sections to the Bogoliubov-de Gennes Hamiltonian (1) from the main text, describing a single band non-centrosymmetric superconductor [38, 39]. First, we note that time-reversal symmetry for $H(\boldsymbol{k})$, Eq. (1), is implemented by $U_T H^*(-\boldsymbol{k})U_T^\dagger = +H(\boldsymbol{k})$ with $U_T = \sigma_0\otimes i\sigma_2$. Hence, we need to set $u_T = i\sigma_2$ in Eq. (A2). It then follows from Eq. (A6) that $H(\boldsymbol{k})$ can be brought into block off-diagonal form by the unitary transformation

$$V = \frac{1}{\sqrt{2}}\begin{pmatrix} \mathbb{1}_2 & -\sigma_2 \\ \mathbb{1}_2 & +\sigma_2 \end{pmatrix}. \tag{D1}$$

The transformed Hamiltonian is given by

$$VH(\boldsymbol{k})V^\dagger = \begin{pmatrix} 0 & D(\boldsymbol{k}) \\ D^\dagger(\boldsymbol{k}) & 0 \end{pmatrix}, \tag{D2}$$

with the off-diagonal block

$$\begin{aligned} D(\boldsymbol{k}) &= \begin{pmatrix} B_{\boldsymbol{k}} + Al_{\boldsymbol{k}}^z & A(l_{\boldsymbol{k}}^x - il_{\boldsymbol{k}}^y) \\ A(l_{\boldsymbol{k}}^x + il_{\boldsymbol{k}}^y) & B_{\boldsymbol{k}} - Al_{\boldsymbol{k}}^z \end{pmatrix} \\ &= B_{\boldsymbol{k}}\sigma_0 + A\,\boldsymbol{l}_{\boldsymbol{k}}\cdot\boldsymbol{\sigma}, \end{aligned} \tag{D3}$$

and where we have introduced the short-hand notation

$$A = \alpha + i\Delta_t, \quad B_{\boldsymbol{k}} = \varepsilon_{\boldsymbol{k}} + i\Delta_s. \tag{D4}$$

Alternatively, we can also choose to work in the basis (A8), in which case the off-diagonal component reads

$$\bar{D}(\boldsymbol{k}) = \begin{pmatrix} A(l_{\boldsymbol{k}}^x - il_{\boldsymbol{k}}^y) & -B_{\boldsymbol{k}} - Al_{\boldsymbol{k}}^z \\ B_{\boldsymbol{k}} - Al_{\boldsymbol{k}}^z & -A(l_{\boldsymbol{k}}^x + il_{\boldsymbol{k}}^y) \end{pmatrix}. \tag{D5}$$

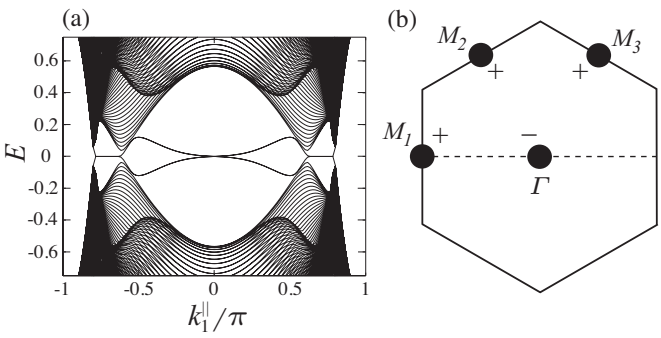

FIG. 5. (a) Band structure of Hamiltonian (1) for the point group O in a slab geometry with (111) face as a function of surface momentum $k_1^{\parallel}$ with $k_2^{\parallel}=0$, i.e., along the dashed line in panel (b). Here, we set $(g_2,\Delta_s)=(0.3,0.5)$. (b) Brillouin zone of the (111) surface with the values of $W_{(111)}(\boldsymbol{K}_{\parallel})$, Eq. (D12), at the four time reversal invariant momenta $\boldsymbol{K}_{\parallel}\in\{\Gamma, M_1, M_2, M_3\}$.

For the computation of the flat band Hamiltonian $Q(\boldsymbol{k})$ it is, however, more convenient to use Eq. (D3).

Repeating the steps of section B, we calcualte the eigenvectors $u_a(\boldsymbol{k})$ of

$$D_{\boldsymbol{k}}D_{\boldsymbol{k}}^\dagger = |A|^2 l_{\boldsymbol{k}}^2 + |B_{\boldsymbol{k}}|^2 + (AB_{\boldsymbol{k}}^* + B_{\boldsymbol{k}}A^*)\boldsymbol{l}_{\boldsymbol{k}}\cdot\boldsymbol{\sigma}, \tag{D6}$$

where $l_{\boldsymbol{k}} = |\boldsymbol{l}_{\boldsymbol{k}}|$. The eigenfunctions $u_a(\boldsymbol{k})$ of $D_{\boldsymbol{k}}D_{\boldsymbol{k}}^\dagger$ can be obtained by diagonalizing $\boldsymbol{l}_{\boldsymbol{k}}\cdot\boldsymbol{\sigma}$. Hence, when $(l_{\boldsymbol{k}}^x, l_{\boldsymbol{k}}^y)\neq(0,0)$, we find that the eigenvectors $u_a(\boldsymbol{k})$ are given by

$$u_{1/2}(\boldsymbol{k}) = \frac{1}{\sqrt{2l_{\boldsymbol{k}}(l_{\boldsymbol{k}}\mp l_{\boldsymbol{k}}^z)}}\begin{pmatrix} l_{\boldsymbol{k}}^x - il_{\boldsymbol{k}}^y \\ \pm l_{\boldsymbol{k}} - l_{\boldsymbol{k}}^z \end{pmatrix}. \tag{D7}$$

According to Eq. (B11), the off-diagonal block of the flat band Hamiltonian $Q(\boldsymbol{k})$ is defined in terms of the eigenvectors $u_a(\boldsymbol{k})$. Thus, we need to compute

$$\begin{aligned} &\sum_{a=1,2}\frac{1}{\lambda_{a\boldsymbol{k}}}u_a(\boldsymbol{k})u_a^\dagger(\boldsymbol{k}) \\ &= \frac{1}{2\lambda_{1\boldsymbol{k}}\lambda_{2\boldsymbol{k}}}\left[(\lambda_{1\boldsymbol{k}}+\lambda_{2\boldsymbol{k}})\sigma_0 + (\lambda_{2\boldsymbol{k}}-\lambda_{1\boldsymbol{k}})\frac{\boldsymbol{l}_{\boldsymbol{k}}}{l_{\boldsymbol{k}}}\cdot\boldsymbol{\sigma}\right], \end{aligned} \tag{D8}$$

with the two positive eigenvalues $\lambda_{1\boldsymbol{k}} = |B_{\boldsymbol{k}} - Al_{\boldsymbol{k}}|$ and $\lambda_{2\boldsymbol{k}} = |B_{\boldsymbol{k}} + Al_{\boldsymbol{k}}|$. Note that the last term in the second line of Eq. (D8) contains removable singularities at the points $\boldsymbol{k}_0$ where $\boldsymbol{l}_{\boldsymbol{k}_0}=0$. For those points in the Brillouin zone one needs to carefully take the limit $\boldsymbol{k}\to\boldsymbol{k}_0$ to obtain the correct value of Eq. (D8). Finally, by use of Eq. (B11) together with Eqs. (D3) and (D8) we find for the off-diagonal block of the flat band Hamiltonian

$$\begin{aligned} q(\boldsymbol{k}) = \frac{1}{2\lambda_{1\boldsymbol{k}}\lambda_{2\boldsymbol{k}}}\Big[&\left\{Al_{\boldsymbol{k}}(\lambda_{2\boldsymbol{k}}-\lambda_{1\boldsymbol{k}}) + B_{\boldsymbol{k}}(\lambda_{1\boldsymbol{k}}+\lambda_{2\boldsymbol{k}})\right\}\sigma_0 \\ &+\left\{Al_{\boldsymbol{k}}(\lambda_{1\boldsymbol{k}}+\lambda_{2\boldsymbol{k}}) + B_{\boldsymbol{k}}(\lambda_{2\boldsymbol{k}}-\lambda_{1\boldsymbol{k}})\right\}\frac{\boldsymbol{l}_{\boldsymbol{k}}}{l_{\boldsymbol{k}}}\cdot\boldsymbol{\sigma}\Big]. \end{aligned} \tag{D9}$$

Now, for the $\mathbb{Z}_2$ invariant we need to bring $q(\boldsymbol{k})$ into the basis in which $U_T = i\sigma_2\otimes\mathbb{1}_2$. This is achieved by letting

$$q(\boldsymbol{k}) \quad\to\quad -iq(\boldsymbol{k})\sigma_2. \tag{D10}$$

Using Eq. (C8) we get

$$W = \prod_{\boldsymbol{K}} \frac{\mathrm{Pf}\,\left[i\sigma_2 q^T(\boldsymbol{K})\right]}{\sqrt{\det\left[i\sigma_2 q^T(\boldsymbol{K})\right]}} = \prod_{\boldsymbol{K}} \frac{B_{\boldsymbol{K}}}{\sqrt{B^2_{\boldsymbol{K}}}}, \quad \text{(D11)}$$

where we have made use of the fact that $\boldsymbol{l}_{\boldsymbol{k}}$ is an antisymmetric function, i.e., $\boldsymbol{l}_{-\boldsymbol{k}} = -\boldsymbol{l}_{\boldsymbol{k}}$.

1. $\mathbb{Z}_2$ surface state

As discussed in the main text, the $\mathbb{Z}_2$ number (D11) can be used to deduce the presence of Andreev surface states at time-reversal invariant momenta of the surface BZ. To exemplify this, let us consider Hamiltonian (1) in a slab geometry with (lmn) face. At the four time-reversal invariant momenta $\boldsymbol{K}_\parallel$ of the (lmn) surface BZ the $\mathbb{Z}_2$ invariant is defined by

$$W_{(lmn)}(\boldsymbol{K}_\parallel) = \prod_{\boldsymbol{K}_\perp} \frac{\mathrm{Pf}\,\left[i\sigma_2 q^T(\boldsymbol{K}_\perp, \boldsymbol{K}_\parallel)\right]}{\sqrt{\det\left[i\sigma_2 q^T(\boldsymbol{K}_\perp, \boldsymbol{K}_\parallel)\right]}}. \quad \text{(D12)}$$

Eq. (D12) is quantized to $+1$ or -1, with $W_{(lmn)}(\boldsymbol{K}_\parallel) = -1$ indicating the presence of Kramers degenerate surface modes at the surface momentum $\boldsymbol{K}_\parallel$ (see Fig. 5).

[26] M. R. Zirnbauer, J. Math. Phys. **37**, 4986 (1996).
[27] A. Altland and M. R. Zirnbauer, Phys. Rev. B **55**, 1142 (1997).
[28] G. E. Volovik, in *The Universe in a Helium Droplet*, The International Series of Monographs on Physics Vol. 117 (Oxford University Press, New York, 2003); G. E. Volovik, in *Exotic Properties of Superfluid 3He*, Series I N Modern Condensed Matter Physics Vol. 1 (World Scientific, Singapore, 1992).
[29] R. Roy, arXiv:0803.2868 (unpublished).
[30] X.-L. Qi, T. Hughes, and S.-C. Zhang, Phys. Rev. B **78**, 195424 (2008).
[31] A. P. Schnyder, S. Ryu, and A. W. W. Ludwig, Phys. Rev. Lett. **102**, 196804 (2009).
[32] A. P. Schnyder, P. M. R. Brydon, D. Manske, and C. Timm, arXiv:1008.3762 (unpublished).
[33] C. Kane and E. Mele, Phys. Rev. Lett. **95**, 226801 (2005).
[34] C. Kane and E. Mele, Phys. Rev. Lett. **95**, 146802 (2005).
[35] L. Fu and C. L. Kane, Phys. Rev. B **76** 045302 (2007).
[36] J. E. Moore and L. Balents, Phys. Rev. B **75** 121306 (2007).
[37] R. Roy, Phys. Rev. B **79**, 195321 (2009).
[38] P. A. Frigeri, D. F. Agterberg, A. Koga, and M. Sigrist, Phys. Rev. Lett. **92**, 097001 (2004).
[39] K. V. Samokhin and V. P. Mineev, Phys. Rev. B **77**, 104520 (2008).